# Distributions of Plasmas and Electric Fields over the Auroral Zones and Polar Caps

L. A. FRANK AND D. A. GURNETT

*Department of Physics and Astronomy*
*University of Iowa, Iowa City 52240*

Simultaneous observations of direct-current electric fields and low-energy charged particles at low altitudes over the earth's auroral zones and polar caps were obtained with the satellite Injun 5. Several of the principal results for several passes of the satellite through the evening and dawn local-time sectors are summarized as follows. (1) The most prominent features of the convection electric fields are reversals located at high magnetic latitudes in the dawn and evening sectors. (2) The east-west convection velocity is usually antisunward at latitudes above the reversal boundary and sunward at latitudes below the reversal boundary. (3) The convection electric-field reversals in the dawn and evening sectors are coincident with the 'trapping boundary' for energetic electrons $E > 45$ kev. This trapping boundary is observationally identified with the high-latitude termination of measurable electron intensities as viewed with a detector with a generous geometry factor. This trapping boundary is not synonymous with the high-latitude limit of durable trapping; i.e., an electron with these energies is not necessarily able to execute a complete longitudinal drift motion. (4) Over the polar caps the convection velocities are small or below the instrumental threshold of typically $\sim$0.75 km $(\text{sec})^{-1}$, relative to the convection velocities in the vicinity of the reversals. (5) The polar-cap region is characterized by an absence of measurable low-energy proton and electron intensities. (6) Inverted 'V' precipitation events, which are characterized by increasing average electron energies to a peak energy and a subsequent decrease in energy as the satellite passes through this intense precipitation event, are located near or at the convection field reversals (and hence also the trapping boundaries) or within regions of measurable convection electric fields poleward of the trapping boundary. (7) Field-aligned electron angular distributions occur at and above the trapping boundary and within the inverted 'V' precipitation events. (8) Diffuse precipitation zones of electron and proton intensities with spectrums similar to those observed in the near-earth plasma sheet are located at latitudes below the trapping boundary and within the region of sunward convection velocities. The ratios of intensities at pitch angles $\alpha = 0°$ to those measured at $\alpha = 90°$ (northern hemisphere) are usually $\lesssim 1$. (9) During a magnetic substorm the over-all configuration of the convection velocities and plasma regions remained similar to those observed during quiescent periods, except that convection velocities and particle intensities increased and the locations of these phenomena in magnetic latitude varied. These observations are interpreted in terms of a magnetospheric model as deduced from plasma observations in the distant magnetosphere and in terms of essential elements for any credible theory of auroral arcs, in particular those associated with inverted 'V' precipitation bands.

Over the past several years it has become increasingly evident that simultaneous observations of the plasmas and electric fields above the auroral zones are necessary to delineate the sources of auroral radiations. The techniques for measuring electric fields, using $Ba^+$ cloud releases [*Haerendel and Lust*, 1970; *Wescott et al.*, 1970] and satellite instrumentation [*Gurnett*, 1970; *Maynard and Heppner*, 1970], have now been introduced successfully. A host of satellites employing a variety of low-energy particle detectors has already provided a survey of the plasmas above the auroral zones. A review of these measurements has been given by *Hultqvist* [1969]. Although measurements of both electric fields and plasmas at low altitudes over the polar caps and auroral zones and within the outer radiation zone are available, theoretical interpretations of such phenomena as auroral arcs are largely conjectural in nature. This situation arises largely owing to the present unavailability of simultaneous observations of

auroral electric fields and plasmas. Our purpose here is to summarize the initial results of such a comparison of electric fields transverse to the local geomagnetic-field vector and of the auroral corpuscular radiation, as measured simultaneously with a low-altitude polar-orbiting satellite.

## Brief Description of Instrumentation

The earth satellite Injun 5 was launched on August 8, 1968, into a near-polar orbit with inclination 81° and apogee and perigee altitudes 2528 and 677 km, respectively. The spacecraft was magnetically aligned with respect to the local magnetic-field vector by means of two parallel bar magnets. A tape recorder with a bit rate of 800 bits $(\text{sec})^{-1}$ provided worldwide surveys of plasma and electric fields. The second telemetry mode, 24,000 bits $(\text{sec})^{-1}$, yielded real-time observations of auroral-zone phenomena with high temporal resolution. Our current interest lies with survey measurements at moderate and high magnetic latitudes in the dawn-dusk meridional plane.

*Low-energy charged-particle detectors.* Simultaneous observations of electron and proton intensities within the energy range $5 \lesssim E \lesssim 50{,}000$ ev were obtained with an array of electrostatic analyzers. A description of this instrumentation has been previously given [*Frank et al.*, 1966]. For this survey we use measurements obtained with two low-energy proton and electron differential energy analyzers (abbreviation, Lepedea), one with fields-of-view directed antiparallel to the local magnetic-field vector (Lepedea 'A') and the other with fields-of-view directed perpendicular to this vector (Lepedea 'B'). Hence Lepedea 'A' measures the precipitated fluxes into the earth's atmosphere over the northern hemisphere. Each of these analyzers provides observations of the directional differential intensities of protons and electrons, separately and simultaneously. In the 'survey' mode of telemetry operation, the instrument sensitivity, temporal resolution, and energy range are sufficient to provide identification of the corresponding plasma regime in the distant magnetosphere, e.g., polar cap, plasma sheet, polar cusp, and proton ring current. Energetic electron intensities with $E > 45$ kev and associated phenomena such as the 'trapping boundary' were determined with a companion set of collimated thin-windowed Geiger-Mueller tubes. For high-spatial and high-temporal resolution studies of auroral phenomena, the reader is referred to the survey given by *Frank and Ackerson* [1971]. However, all observations presented here were gathered in the survey mode, which permitted surveys over entire orbits via the satellite tape recorder and allowed us to establish the connections between the plasma phenomena and convection electric fields on a global scale at low altitudes.

*dc electric-field instrumentation.* The dc electric-field instrumentation has been described by *Gurnett et al.* [1969] and initial results have been presented by *Gurnett* [1970] and *Cauffman and Gurnett* [1971]. The electric-field sensor consists of two conducting spheres mounted on booms with a center-to-center separation of 2.85 meters. The electric-field component parallel to the axis through the spheres is determined by measuring the potential difference between the spheres with a high-impedance voltmeter. The magnetic orientation of the satellite maintains the electric antenna axis perpendicular to the local geomagnetic-field vector, and thus only the electric-field component perpendicular to the geomagnetic field is sensed.

To determine the electric field due to magnetospheric plasma convection, the $\mathbf{V}_s \times \mathbf{B}$ electric field caused by the satellite motion through the ionosphere and small instrumental errors (due to asymmetrical sunlight shadowing of the spheres by the supporting booms) must be subtracted from the measured electric field. The detailed procedures used to determine this subtracted electric field are discussed by *Cauffman and Gurnett* [1971]. Since sunlight shadowing errors, which cannot be calculated directly, vary slowly with the rotation of the satellite, the accuracy with which the convection electric field can be determined depends on the time, or distance, scale of the phenomena. The rotation period of the spacecraft, and thus also of the electric antenna axis, around the local magnetic-field vector is typically 20 min or longer. For distance scales of 1000 km or less, variations in the convection electric field can be determined with an accuracy $\pm 10$ mv $(\text{m})^{-1}$, or less, whereas over longer distance scales, 5000 km or greater, the accuracy of determination of the absolute convection electric field is normally limited to approximately $\pm 30$ mv $(\text{m})^{-1}$.

## OBSERVATIONS

Two series of observations are presented here, one series for the northern and southern hemispheres during a period of relative magnetic quiescence and the second an example of plasma and electric-field phenomena during a magnetic substorm. We have selected these passes on the basis of telemetry coverage at high latitudes, a dawn-dusk local-time zone for the orbit and relative magnetic activity.

*Period of relative magnetic quiescence* ($Kp = 1^+$). Simultaneous observations of dc electric fields, energetic electron ($E > 45$ kev) intensities, and lower-energy electron ($1.6 \leq E \leq 2.5$ kev) intensities for a northern polar pass on February 7, 1969, are shown in Figure 1. The observations for the following southern polar pass are summarized in Figure 2. Magnetic local times MLT and invariant magnetic latitudes $\Lambda$ as functions of universal time for these two polar passes are available in Figure 3.

The dc electric-field measurements, including the $\mathbf{V}_s \times \mathbf{B}$ field and uncorrected for any shadowing errors, are shown in the top panels of Figures 1 and 2. The systematic sinusoidal variation of the dc electric field with a period of approximately 22 min reflects the previously mentioned rotation of the satellite in the $\mathbf{V}_s \times \mathbf{B}$ field. With the exception of the small perturbation labeled 'spacecraft body shadow,' the deviations from the smooth sinusoidal $\mathbf{V}_s \times \mathbf{B}$ field are due to convection electric fields. The dashed lines in regions where significant convection electric fields are observed is the estimated $\mathbf{V}_s \times \mathbf{B}$ field and represents the 'zero reference' for determining the magnitude and sign of the convection electric-field component detected. Because of the previously mentioned sunlight shadowing errors, the uncertainty in determining the $\mathbf{V}_s \times \mathbf{B}$ field on these orbits is about $\pm 30$ mv $(\text{m})^{-1}$.

The principal features of the dc electric-field observations of Figures 1 and 2 are the abrupt reversals of these electric fields at 1533 and 1641 UT (magnetically conjugate points at local dawn) and the smaller less definitive reversals at about 1543 and 1627 UT (local evening). As discussed by *Cauffman and Gurnett* [1971], this electric-field reversal is associated with a reversal in the generally east-west direction of the plasma convection, with the convection velocity directed sunward on the low-latitude side of the reversal boundary and antisunward on the high-latitude side. Over the polar-cap region at latitudes above the reversal boundary, e.g., for the period 1536 to 1539 UT of Figure 1, the convection electric field is generally small, $\lesssim 0.75$ km $(\text{sec})^{-1}$, as compared with the convection electric fields observed near the reversal boundary.

In a following section we invoke simultaneous measurements of proton and electron intensities to identify the regions, such as plasma sheet and polar cap, in the distant magnetosphere that correspond to the convection zones discussed above. However, we have included observations of electron ($E > 45$ kev) intensities with pitch angles $\alpha = 90°$ in the middle panels of Figures 1 and 2 and of lower-energy electron ($1.6 \leq E \leq 2.5$ kev) intensities in the bottom panels. The energetic electron ($E > 45$ kev) intensity profiles provide a definitive determination of the trapping boundaries at high latitudes. Observationally these boundaries are to be identified with the high-latitude termination of measurable electron intensities, e.g., at approximately 1627 and 1641 UT of Figure 2. The geometric factors of the Geiger-Mueller tubes used to obtain these observations are large, $\sim 0.02$ cm$^2$ ster, relative to those we have employed on previous satellites, and thus they respond to relatively low intensities. We associate this trapping boundary as being coincident with the boundary between magnetic-field lines closed within the magnetosphere (lower latitudes) and open-field lines (higher latitudes) to the interplanetary medium. We will later reject the alternative interpretation invoking closed but unpopulated field lines over the polar cap with measurements of the low-energy particle distributions. These energetic electron intensities near the boundary are not necessarily durably trapped in the sense that an electron populating these higher-latitude closed-field lines will complete a longitudinal drift motion around the earth. With regard to the convection electric field, this trapping boundary almost invariably is coincident with the reversal of the convection from sunward (lower latitude) to antisunward flow at higher latitudes. The observations of Figures 1 and 2 provide prominent examples of the striking correlation of these two phenomena.

Intensities of lower-energy electrons, $1.6 \leq$

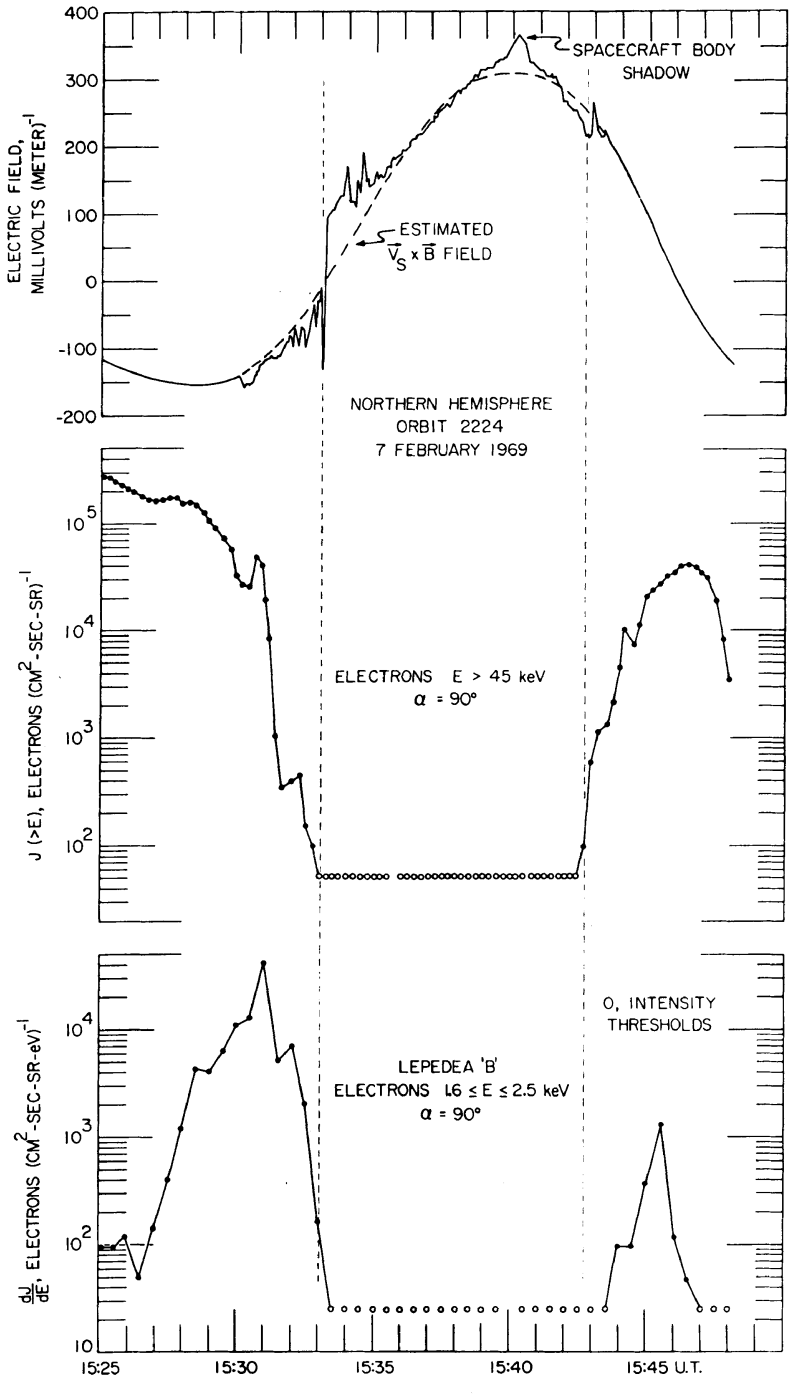


Fig. 1. Simultaneous observations of dc electric fields due to magnetospheric plasma convection and of electron intensities over the northern auroral zone and polar cap on February 7, 1969. The $\mathbf{V_s \times B}$ field is the electric field attributed to the satellite motion through the earth's magnetic field. This period of observations for the dawn and evening local-time sectors was characterized by relative magnetic quiescence ($Kp = 1^+$). The altitudes of the spacecraft at 15h 33m 00s and at 15h 42m 45s were 1483 and 1029 km, respectively.

$E \leq 2.5$ kev, at local pitch angle $\alpha = 90°$ are shown in the bottom panels of Figures 1 and 2. This energy range and pitch angle were chosen as a coarse index to the regions of electron precipitation into the northern and southern auroral zones. Over the northern hemisphere, these electron events were confined to latitudes within the outer radiation zone and were located equatorward of the trapping boundary. Inspection of the responses of the analyzers for other energy bandpasses provides identification of these precipitation events as the diffuse struc-

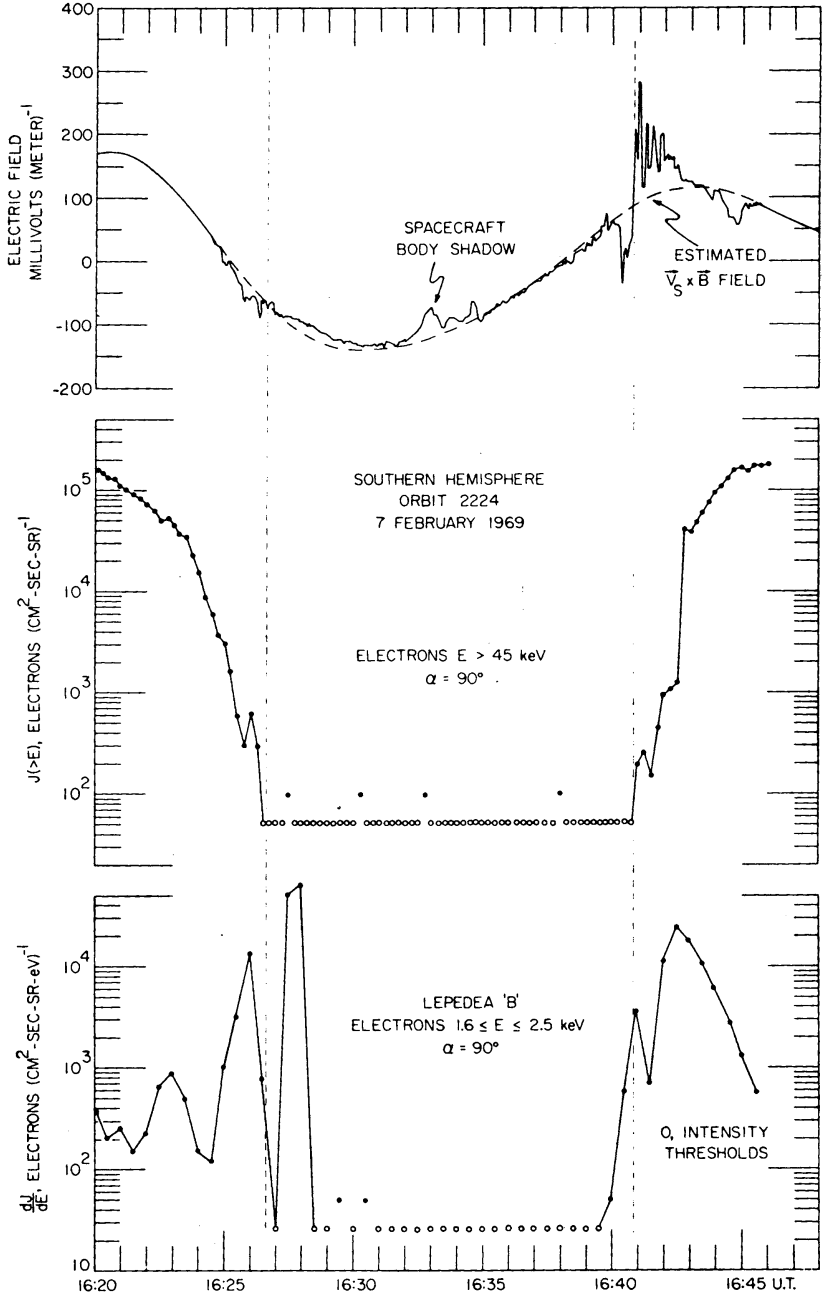


Fig. 2. Continuation of Figure 1 for the following southern polar pass approximately 1 hour later. The altitudes of the spacecraft at 16h 26m 35s and at 16h 40m 50s were 1707 and 2291 km, respectively.

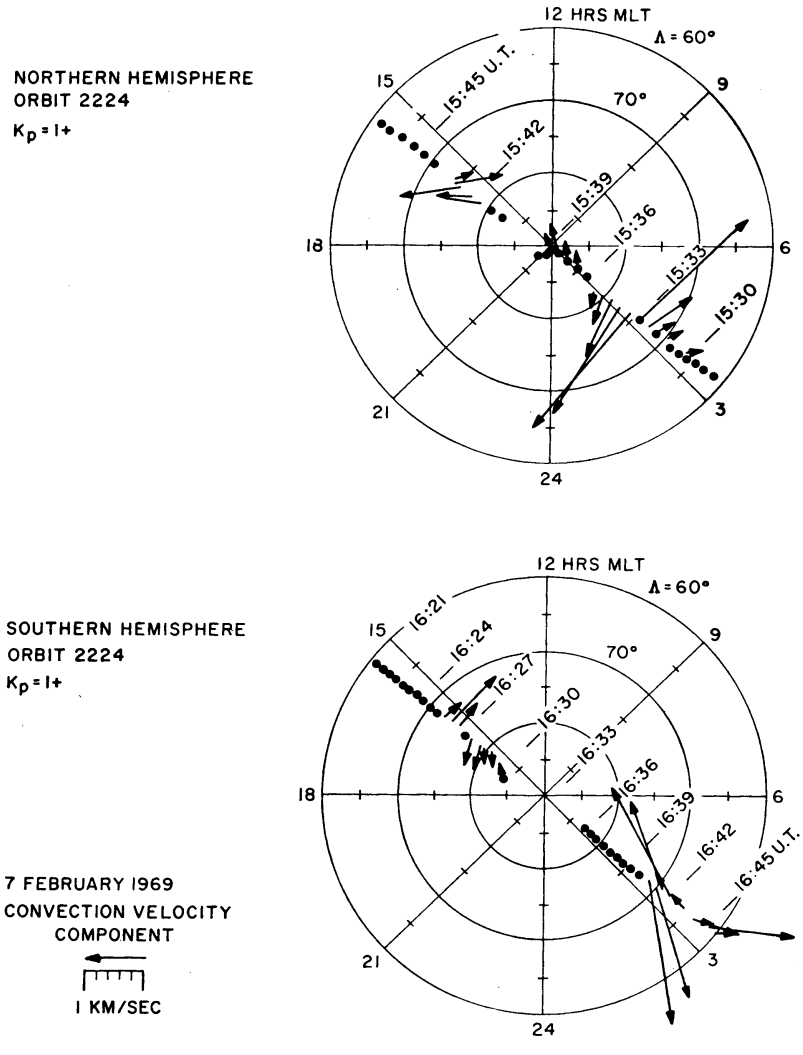


Fig. 3. Polar diagram for the convection velocity component of the electric-field observations displayed in Figures 1 and 2. The coordinates are magnetic local time (MLT) and invariant latitude (Λ).

tureless type with relatively hard electron spectrums observed at these local times, as previously discussed by *Frank and Ackerson* [1971]. The observations over the southern polar cap revealed a similar type of hard electron precipitation equatorward of the trapping boundary, with the exception of the two maximums of intensities centered at 1628 and 1641 UT located near the trapping boundary and convection electric-field reversals.

These two maximums of intensities are the signatures of a second type of precipitation event discussed by *Frank and Ackerson* [1971], the inverted 'V' electron precipitation event. These intense events are characterized by (*a*) rapidly decreasing differential intensities with increasing electron energy in the high-energy tail of the spectrum (soft spectrum), (*b*) widths typically ~50 to 300 km, and (*c*) average electron energy that rises from $\lesssim$100 ev to a maximum energy ranging from approximately several hundred electron volts to tens of kiloelectron volts and returns to $\lesssim$100 ev with the passage of the satellite through the precipitation band (evidenced by an inverted 'V' structure in energy-time spectrograms of these events).

Again the reader is referred to the survey given by *Frank and Ackerson* [1971] for examples of these two types of precipitation events. Intense soft electron events were also observed near the trapping boundaries for the northern polar pass of Figure 1. However, the peak energies of the inverted 'V' substructure were low, approximately several hundred electron volts, and there were no electron ($1.6 \leq E \leq 2.5$ kev) intensities exceeding the detector threshold intensity. We expand our discussion of the relationships of these precipitation events with respect to auroral and magnetospheric phenomena with the presentation of results obtained during a period of magnetic activity.

A further useful summary of the convection velocity components and the orbit for the series of measurements of Figures 1 and 2 is given in the polar diagram of magnetic local-time invariant latitude (MLT — $\Lambda$) of Figure 3. Since only one component of the electric field is sensed, only the component of convection velocity perpendicular to the axis of the electric antenna can be determined. The direction of the arrows in Figure 3 is in the direction of the convection velocity sensed, and the length of arrows is proportional to the magnitude of this velocity as computed from $V_c = E_c/B$, where $E_c$ is the convection electric field obtained after subtracting the $\mathbf{V_s \times B}$ field and shadowing errors from the measured electric field and $B$ is the scalar value of the local geomagnetic field. It must be emphasized that the arrow represents only the component of the convection velocity detected; it does not represent the vector direction of the convection velocity, since only one component is measured.

The electric-field reversal at 1533 UT in Figure 1 corresponds to the reversal in the east-west convection velocity shown in the dawn sector of the northern-hemisphere polar diagram of Figure 3. The reversal in the east-west convection in this region is particularly clear here because the electric antenna was aligned approximately north-south at this time and was measuring the east-west component of the convection velocity. On the high-latitude side of the reversal, above the trapping boundary for energetic electrons (see Figure 1), the plasma convection is westward, away from the sun, and on the low-latitude side of the reversal, equatorward of the trapping boundary, the convection velocity is eastward, toward the sun. In the southern hemisphere the magnetically conjugate reversal at 1641 UT is qualitatively the same, although the antenna orientation is not as favorable for detecting east-west convection.

The smaller reversals on the duskside of the polar region at 1543 and 1627 UT are also consistent with respect to the east-west component of the convection velocity in opposite hemispheres; with antisunward convection poleward of the trapping boundary and sunward convection equatorward of the trapping boundary.

The convection velocities shown in the polar diagram of Figure 3, although somewhat larger in magnitude than usually observed, illustrate several features frequently displayed by the convection velocities observed in the dawn-dusk sectors with Injun 5: (*a*) the east-west convection velocity is antisunward at latitudes above the reversal boundary and sunward at latitudes below the reversal boundary, (*b*) the convection velocity over the polar region is small compared to the convection velocities observed in the reversal region, and (*c*) the reversal is larger in magnitude and better defined in the dawn sector and smaller and less definitive in the dusk region.

*Observations during a magnetic substorm* ($Kp = 3^-$). Measurements of the electric fields and particle intensities over the northern hemisphere during a polar magnetic substorm on March 13, 1970, are summarized in Figure 4. The magnetograms acquired at College, Alaska, clearly show that a moderate magnetic substorm was in progress during these satellite observations while the magnetic observatory was located in the postmidnight local-time sector. As we will see, the over-all interrelationships of the various phenomena observed during these magnetic disturbances do not differ in character from the findings for the periods of relative magnetic quiescence presented above; the primary difference is evident in the magnitudes and position in latitude of the electric field and plasma phenomena. This series of observations was also selected for analysis, in addition to magnetic activity, because of the slow rotation rate of the satellite (~1 hour) and the favorable (approximately north-south) orientation of the electric-field antenna for detecting the east-west component of the plasma

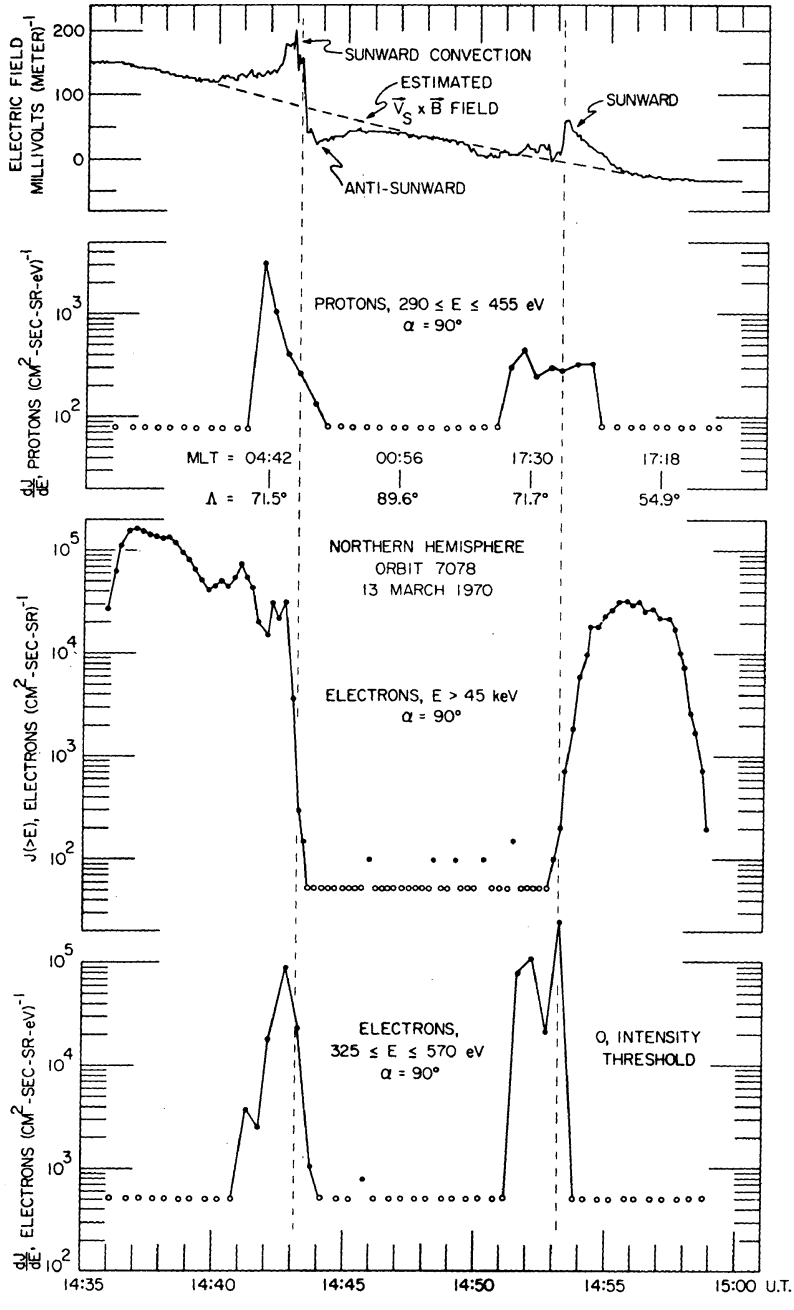


Fig. 4. Simultaneous observations of proton and electron intensities at local pitch angle $\alpha = 90°$ and of dc electric fields for a northern polar pass on March 13, 1970. With increasing universal time, the satellite passed over the auroral zone at local dawn and over the polar-cap region and the auroral zone at local evening. A moderate substorm was in progress as evidenced in the magnetograms obtained at College, Alaska, which was in the post-midnight sector. The magnetic index $Kp = 3^-$. The altitudes of the spacecraft at 14h 43m 05s and at 14h 53m 05s were 693 and 824 km, respectively.

convection. The measurements of Figure 4 begin in the dawn local-time sector and continue into the polar-cap region and then into local evening. A summary of the satellite position in MLT-Λ polar coordinates is found in Figure 5.

The dc electric-field measurements obtained during this pass display a large electric-field reversal at 1443 UT in the dawn local-time sector and a smaller discontinuity at 1453 UT in the local evening sector. Owing to the slow rotation of the satellite aud the complete absence of sunlight shadowing errors, the convection electric field can be determined with exceptionally good accuracy during this pass, $\sim\pm 10$ mv $(m)^{-1}$. Over the polar-cap region, which was encountered from approximately 1446 to 1450 UT, the convection electric field is essentially zero within the resolution of the measurements. The latitudinal width of the polar-cap region is $\sim 12°$ and its midpoint is displaced toward local evening relative to the northern magnetic pole (see Figure 5). The convection velocity components are also summarized in Figure 5. The east-west convection velocities observed during this pass are qualitatively similar to the convection patterns observed for the magnetically quiescent period discussed earlier, except that the reversal regions are broader and the convection velocities are enhanced during the substorm.

The trapping boundary for energetic electron ($E > 45$ kev) intensities is coincident with the

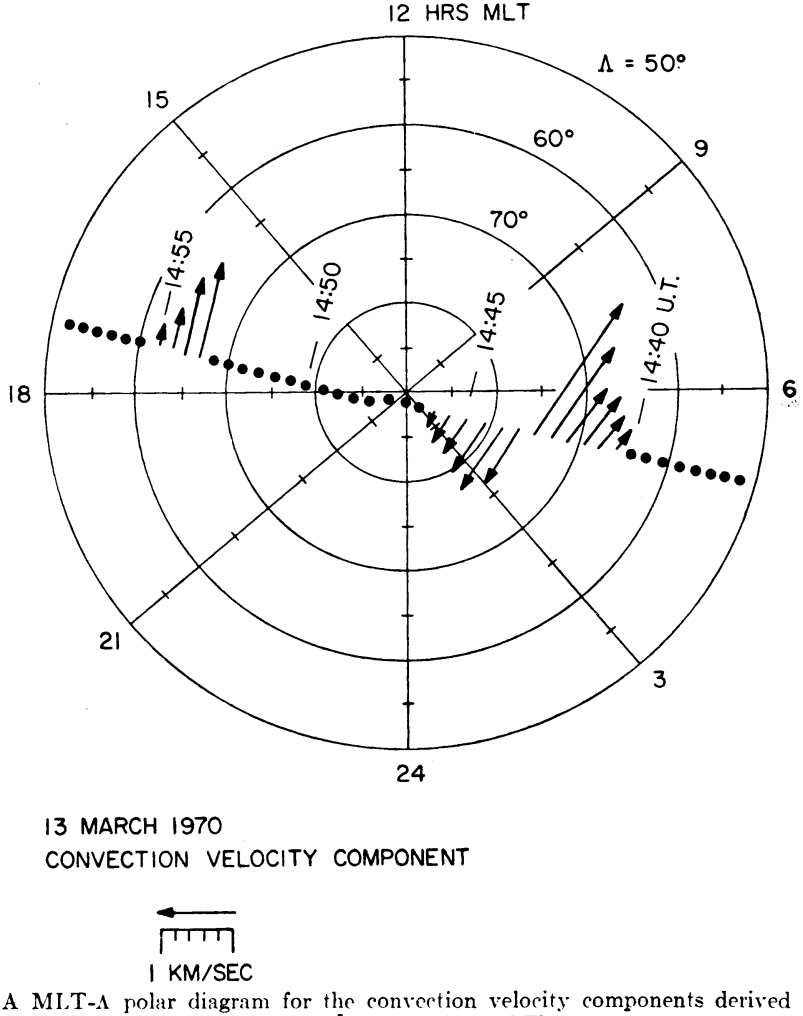


Fig. 5. A MLT-Λ polar diagram for the convection velocity components derived from the dc electric field observations of Figure 4.

two major reversals at 1443 and 1453 UT, as was found for the period of relative magnetic quiescence. This correlation is clearly discernible in Figure 4.

Low-energy proton ($290 \leq E \leq 455$ ev) intensities (second panel from top of Figure 4) are located poleward and equatorward of the trapping boundary in the dawn and dusk local-time sectors. These proton intensities will be identified here via their energy spectrums according to their association with the high-latitude magnetotail (distant plasma sheet) and the near-earth plasma sheet [see *Frank*, 1970*a*; *Frank and Ackerson*, 1971].

Electron ($325 \leq E \leq 570$ ev) intensities provide a useful index of the location of inverted 'V' precipitation events. These measurements are summarized in the bottom panel of Figure 4. Like observations during magnetic quiescence, these events are located near or at the position of the trapping boundaries and electric-field reversals at 1443 and 1453 UT. The second, or poleward, precipitation event at 1452 UT of the pair of evening inverted 'V' events is also located in a region of measurable antisunward convection.

The observations over the polar cap itself for both quiescent and disturbed magnetic conditions presented here feature an absence of measurable low-energy charged-particle intensities and relatively weak convection electric fields (see Figures 1, 2, and 4). A similar absence of measurable particle intensities in the polar-cap region of the distant polar magnetosphere has been recently reported by *Frank* [1971*a*].

Measurements of low-energy charged-particle intensities within a few energy bandpasses like those shown in Figures 1, 2, and 4 are adequate for a coarse determination of the location of major precipitation zones. However, the full capabilities of the analyzer array must be employed to identify positions for field-aligned currents, hard and soft precipitation zones, and protons of the plasma sheet. Such an analysis for the substorm observations of Figure 4 is presented in the block diagram of Figure 6. This diagram is a comprehensive road map for the various regions and plasma phenomena encountered during this northern polar pass. A summary of the nature of the convection electric fields is shown at the top of Figure 6. The charged-particle phenomena are summarized in the bottom half of this diagram.

(*a*) Electron $E > 45$ kev trapping boundary, the high-latitude termination of measurable intensities of electrons $E > 45$ kev.

(*b*) Proton spectrums, classified 'hard' or 'soft' on the presence or absence, respectively, of measurable intensities of protons $E > 10$ kev.

(*c*) Electron spectrums, classified 'hard' or 'soft' with the absence or presence, respectively, of large intensities of lower-energy electrons, $50 \lesssim E \lesssim 400$ ev. (The soft spectrums are also characterized by a relatively rapid decrease of differential electron intensities with decreasing electron energy in the high-energy tail of the spectrum; see also *Frank and Ackerson* [1971].)

(*d*) Electron angular distributions: $j(0°)/j(90°) \lesssim 1$, maximum intensities at pitch angle $\alpha = 90°$; or $j(0°)/j(90°) \gtrsim 1$, field-aligned current directed out of the atmosphere assuming no significant upflux (see K. L. Ackerson and L. A. Frank, unpublished manuscript, 1971).

(*e*) Electron inverted 'V' events, bands of electron precipitation characterized by average electron energies rising from $\lesssim$100 ev to a maximum energy typically ranging from several hundred electron volts to tens of kiloelectron volts and returning to $\lesssim$100 ev with the passage of the satellite through this precipitation event (for examples of these intense events, see *Frank and Ackerson* [1971]).

(*f*) Plasma region in distant magnetosphere: polar cap, identified by absence of measurable low-energy proton and electron intensities and of detectable convection electric fields; polar cusp and distant plasma sheet (high-latitude magnetotail and downstream magnetosheath), identified by presence of soft proton and electron spectrums, antisunward convection and local-time sector [*Frank*, 1970*a*, 1971*a*] and near-earth plasma sheet, located equatorward of the trapping boundary and identified with measurable intensities of energetic electrons $E > 45$ kev and sunward convection, includes regions of hard proton and electron spectrums and is usually bounded at its poleward side by inverted 'V' events. The signature of this region at low altitudes includes the ring current at low magnetic latitudes and the plasma sheet proper

at geocentric radial distances $\gtrsim 20\ R_E$ at the higher latitudes.

We summarize all of the observational results in the next section. However, although many features of this road map are obvious, we cite the asymmetric injection of ring current protons into the local evening sector as an example. The satellite transit time from the low-latitude edge of the extraterrestrial ring current at 14h 41m 10s UT in the local morning sector to the corresponding position in the local evening sector at 14h 55m 40s UT was only ~15 min. These two boundaries were located at $\Lambda = 68.4°$ and 59.3° in the morning and evening sectors, respectively; the corresponding $L$ values were $L = 7.3$ and 3.8. A similar asymmetry was encountered during the following southern pass, approximately 1 hour later. This asymmetric injection of proton intensities to $L$ values deep within the outer radiation zone at local evening during magnetic substorms is similar to the one reported by *Frank* [1970*b*] utilizing measurements of proton intensities near the magnetic equatorial plane.

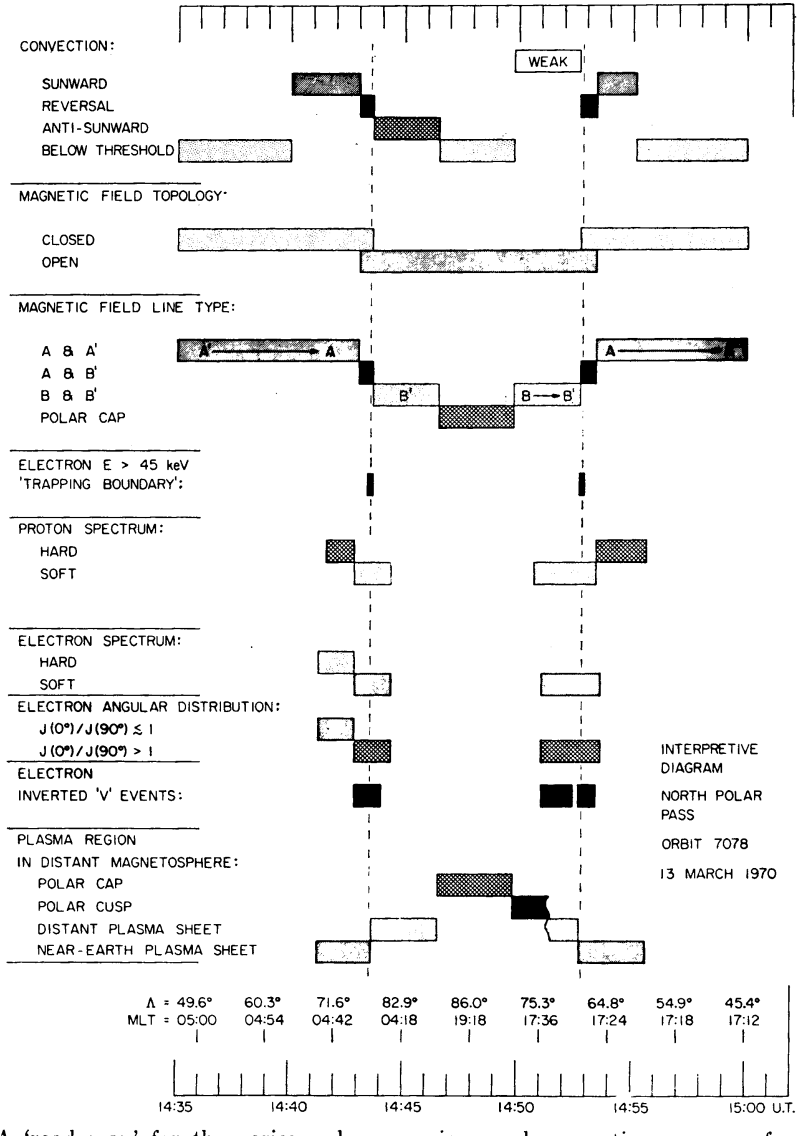


Fig. 6. A 'road map' for the various plasma regions and convection zones as functions of universal time for observations during the northern polar pass of Figure 4.

## SUMMARY OF OBSERVATIONS

Several examples of simultaneous plasma and dc electric-field measurements at low altitudes over the earth's polar caps and auroral zones have been presented. These observations were obtained in the dawn and evening local-time sectors. For the convenience of the reader, we summarize here the principal observational results.

1. The most prominent features of the convection electric fields are reversals located at high magnetic latitudes in the dawn and evening sectors (see Figure 2 at approximately 1627 and 1641 UT).

2. The east-west convection velocity is usually antisunward at latitudes above the reversal boundary and sunward at latitudes below the reversal boundary (see Figure 3).

3. The reversal is usually larger and more definitive in the dawn sector and relatively small and less definitive at local evening (see Figures 1 and 3).

4. The convection electric-field reversals in the dawn and evening sectors are coincident with the trapping boundary for energetic electrons $E > 45$ kev. This trapping boundary is observationally identified with the high-latitude termination of measurable electron intensities as viewed with a detector with generous geometry factor. Examples of this trapping boundary are shown at 1533 and 1543 UT of Figure 1; this trapping boundary is not synonymous with the high-latitude limit of durable trapping, i.e., an electron with these energies is not necessarily able to execute a complete longitudinal drift motion.

5. Over the polar caps the convection velocities are generally small or below the instrumental threshold of $\sim$0.75 km $(\text{sec})^{-1}$ for Figure 3 and $\sim$0.25 km $(\text{sec})^{-1}$ for Figure 5, relative to the convection velocities in the vicinity of the reversals (see Figures 3 and 5).

6. The polar-cap region proper is $\sim 10°$ to $20°$ in latitudinal width, lies above the zone of antisunward convection, and is not necessarily centered at the magnetic pole but may be displayed toward local dawn or evening (see Figures 3 and 5).

7. The polar-cap region is characterized by an absence of measurable low-energy proton and electron intensities (see Figures 1, 2, 4, and 6).

8. Inverted 'V' precipitation events, which are characterized by increasing average electron energies to a peak energy and a subsequent decrease in energy as the satellite passes through this intense precipitation event, as discussed by *Frank and Ackerson* [1971], are located near or at the convection field reversals (and hence also the trapping boundaries) or within regions of measurable convection electric fields poleward of the trapping boundary (see Figures 4 and 6).

10. Proton and electron energy spectrums observed at latitudes above the trapping boundary are soft, relative to the spectrums measured equatorward of the trapping boundary (see Figures 4 and 6).

11. Diffuse precipitation zones of electron and proton intensities with spectrums similar to those observed in the near-earth plasma sheet are located at latitudes below the trapping boundary and within the region of sunward convection velocities (see Figures 1 and 6). The ratios of intensities at pitch angles $\alpha = 0°$ to those measured at $\alpha = 90°$ (northern hemisphere) are usually $\lesssim 1$.

12. During a magnetic substorm the over-all configuration of the convection velocities and plasma regions remained similar to those reported here for quiescent periods except that convection velocities and particles intensities increased and the locations of these phenomena in magnetic latitude varied (see Figures 4, 5, and 6).

13. During the substorm the asymmetric injection of protons deep into the outer radiation zone to $L = 3.8$ during local evening was observed. The lowest $L$ value for measurable proton intensities as measured 15 min of elapsed time earlier in the local morning sector was $L = 7.3$.

The above comments summarize the principal observational features of the plasmas and electric fields observed over the earth's polar caps and auroral zones for several passes selected on the basis of telemetry coverage at high latitudes, a dawn-dusk local-time zone, and relative magnetic activity. These results for several, though detailed, examples should not be misinterpreted as the product of a statistical analysis. For example, instances have been found for which large convection velocities, $\gtrsim 1$ km $(\text{sec})^{-1}$, are observed along the entire satellite trajectory

over the polar cap, in contrast to the observations shown in Figure 4. We intend to extend this investigation to include other polar configurations, local-time sectors, and magnetic conditions as soon as possible.

## INTERPRETATION AND DISCUSSION

Over the past few years several models of magnetospheric convection have been proposed to account for polar and magnetospheric substorms. A review of these models has been given by *Axford* [1969]. In our present interpretation of the observational features of convection patterns at low altitudes over the earth's auroral zones and polar caps and of the plasmas in the distant magnetosphere and at low altitudes, we cannot directly invoke such models as *Dungey*'s [1961, 1968], which predict uniform convection of magnetic-field lines over the earth's polar caps. Although we retain here Dungey's concept of the connection of geomagnetic-field lines with those of the interplanetary medium as an important element of any magnetospheric model, several prominent observational features that are inconsistent with the topology of such models are (*a*) strong sunward convection below the trapping boundary for energetic electrons and strong antisunward convection in a zone lying above this boundary and relatively small convection over the polar cap at low altitudes, (*b*) the over-all absence of low-energy magnetosheath protons and electrons over the earth's polar caps, and (*c*) the character of the direct entry of magnetosheath plasma into the dayside magnetosphere and the barren nature of the distant polar-cap region with regard to its population of low-energy proton and electron intensities [*Frank*, 1971*a*].

A magnetospheric model based on observations of low-energy charged particle intensities in the distant polar magnetosphere and near the magnetic equatorial plane has been recently proposed by *Frank* [1971*a*, *b*]. The convection electric fields and over-all character of the charged-particle distributions encountered at low altitudes over the polar caps and auroral zones, as reported here, are in qualitative agreement with this model. A diagram of the pertinent elements of this magnetospheric model is shown in Figure 7. Magnetic merging along the sunlit magnetopause allows the direct entry of magnetosheath plasma into the magnetosphere via the polar cusps. Polar-cusp field lines $B$ and $b$ are connected to interplanetary-field lines in the magnetosheath. Field lines $B$ and $b$ within the polar cusps are convected in the antisolar direction into the distant plasma sheet (magnetic-field lines $B'$ and $b'$). Magnetic-field lines threading the distant plasma sheet extend into the downstream magnetosheath. Merging at the neutral sheet in the magnetotail provides the closed-field lines $A$ within the near-earth plasma sheet. These field lines are convected sunward toward the sunlit magnetopause. Not all field lines of the type $B'$ and $b'$ in the distant plasma sheet merge in the magnetotail. The alternative history of these field lines is to be vacated of magnetosheath plasma as the plasma flows downstream from the earth and subsequently to become polar-cap field lines. The convection patterns expected over the polar caps have been discussed by *Frank* [1971*b*]. The model predicts low convection velocities relative to those at the polar-cusp intersection with the ionosphere (see Figures 3 and 5). Magnetic-field lines $B'$ and $b'$ of the distant plasma sheet lie at latitudes above those of the near-earth plasma sheet $A$ (see 'interior field configuration' of Figure 6); these field lines at geocentric radial distances $\sim$10 to 30 $R_E$ have also been called the 'high-latitude' magnetotail. The energy spectrums of proton and electron intensities in the polar cusp, distant plasma sheet, and high-latitude magnetotail are soft relative to those of the near-earth plasma sheet [see *Frank*, 1970*a*, 1971*a*; *Frank and Ackerson*, 1971]. Electron number densities within the inverted 'V' precipitation events at the trapping boundary are typically $\sim$10 $(cm)^{-3}$, similar to the electron densities in the magnetosheath and larger by factors $\sim$30 than corresponding densities in the near-earth (hard spectrum) plasma sheet at 20 to 30 $R_E$. K. L. Ackerson and L. A. Frank (unpublished manuscript, 1971) have recently proposed that the proton and electron intensities of the near-earth plasma sheet are the 'debris' from inverted 'V' electron events located at the trapping boundary.

For the reader's orientation we consider the implications of this magnetospheric model concerning the phenomena encountered with a low-altitude polar-orbiting satellite. We return to Figure 6 and consider the simplest example, a satellite pass at the local noon meridian. If the

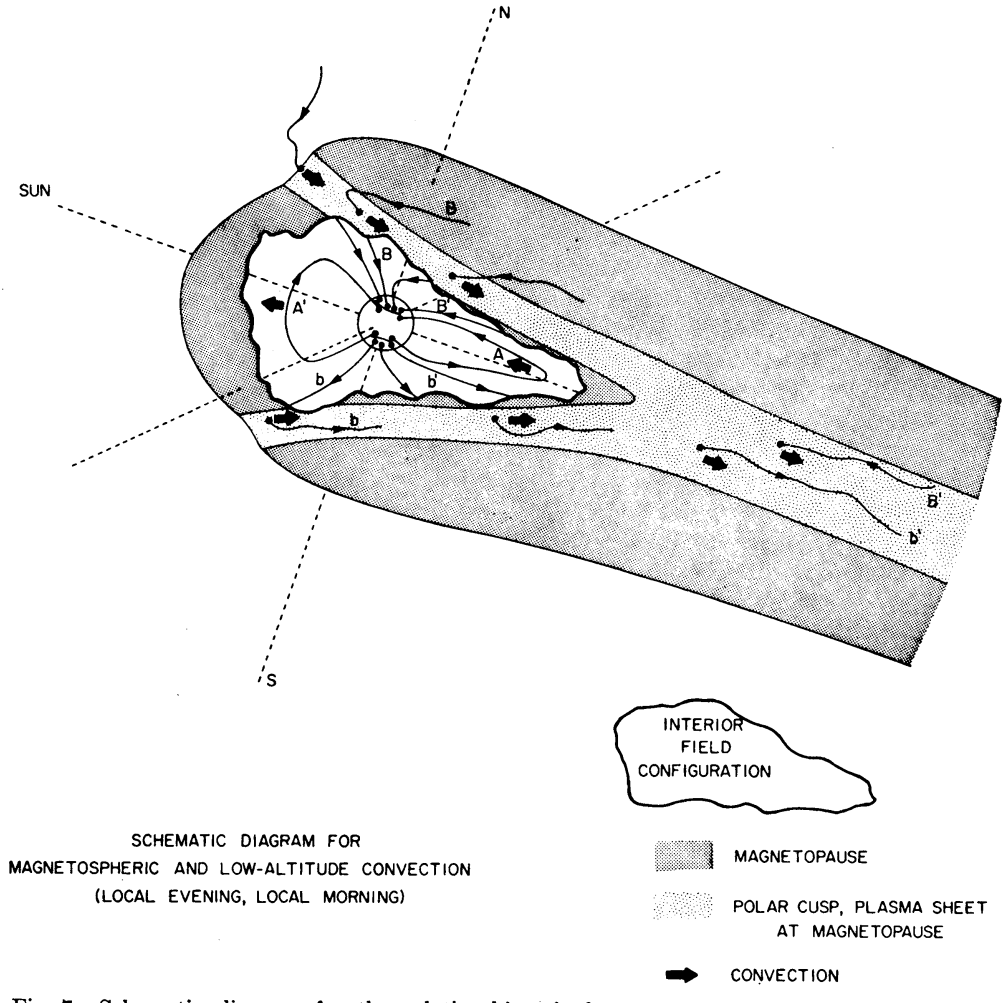


Fig. 7. Schematic diagram for the relationship of plasma and convection regions at low altitudes with the topology and plasma regimes of the distant magnetosphere. (See text.)

satellite is moving equatorward from the polar-cap region, it will first encounter the polar cusp ($B$ and $b$) and enter the inner magnetosphere ($A'$). For a pass at local midnight, the satellite will pass from the polar-cap region, into the high-latitude magnetotail ($B'$ and $b'$), and then into the near-earth plasma sheet ($A$). Similar passes at local morning and evening are topologically somewhat more complex but are directly pertinent to the observations reported here. A satellite pass from the polar-cap region equatorward in these local-time zones will pass in sequence through the polar-cap region, the polar cusp ($B$ and $b$), and/or the distant plasma sheet ($B'$ and $b'$) and finally into the near-earth plasma sheet ($A$).

We have examined a series of low-altitude passes for low-energy proton intensities in the polar-cusp region and its topological extension into the magnetotail, the distant plasma sheet, and we find that the maximum intensities of these magnetosheath protons occur over the sunlit ionosphere. Corresponding intensities in the distant plasma sheet are considerably less. The detailed study of these distributions will be published soon. The spatial distributions of magnetosheath proton intensities are qualitatively in agreement with those deduced by *Eather and Mende* [1970] from photometric surveys. The various plasma regimes in the distant magnetosphere and the magnetic-field-

line types for the substorm observations of Figures 4 and 5 are summarized in Figure 6.

As noted previously by *Frank and Ackerson* [1971], maximum energy fluxes precipitated into the earth's atmosphere frequently occur in the center of an inverted 'V' precipitation event. We associate these intense bands of electron precipitation with auroral arcs, and our following comments are directed toward further pursuing the mechanisms and conditions responsible for these precipitation events. A detailed description of correlated measurements of these electron precipitation events and a ground-based observation of an auroral arc is given by K. L. Ackerson and L. A. Frank (unpublished manuscript, 1971).

These inverted 'V' precipitation events are located in regions of relatively large convection electric fields at or poleward of the trapping boundary. Returning to the electric-field reversal at local dawn shown in Figures 4 and 5, we note that the electric antenna axis was aligned approximately north-south, parallel to the satellite velocity vector, and thus the electrostatic potential $\Phi$ in the reversal region can be determined from the electric field $E$,

$$\Phi = -\int E\, ds$$

where $ds$ is an element of length along the satellite trajectory. This method of determining the electrostatic potential is valid only if the electric-field variations are primarily spatial, as is expected for the electric-field observations shown in Figure 4.

The north-south component of the electric-field reversal in the local-dawn sector during a substorm as shown in Figure 4 is displayed in the bottom panel of Figure 8. The $\mathbf{V}_s \times \mathbf{B}$ field due to the satellite motion along its trajectory has been subtracted. The electrostatic potential obtained by integrating the convection electric field along the satellite trajectory is shown in the middle panel of Figure 8. We have arbitrarily chosen the zero of the electrostatic potential curve as located at 1440 UT, when the spacecraft was at the lowest latitude for detection of a convection electric field. At the time $t_r$ for the encounter of the electric-field reversal at 14h 43m 20s UT, the electrostatic potential reaches a maximum of +56 kv.

Observations of the low-energy proton and electron intensities and their relationship to such phenomena as the trapping boundary and the plasma regimes of the distant magnetosphere are summarized in the top panel of Figure 8 and in Figure 6. The high-latitude boundary of the near-earth plasma sheet is chosen to coincide with the position of the trapping boundary. However, the character and directions of the convection electric fields and the penetration of low-energy plasma equatorward of the trapping boundary in a narrow zone that is $\sim 1°$ in latitudinal width and centered at 14h 43m 20s UT is interpreted here as implying that the boundary between open and closed magnetospheric-field lines is not sharply defined (see Figures 4 and 6). In other words, it appears that this narrow zone comprises both open- and closed-field lines and is topologically mapped into a relatively broad region of reconnection of magnetic-field lines, $\gtrsim 10\ R_E$, along the neutral sheet in the magnetotail.

The most prominent feature of the auroral electron precipitation event is the inverted 'V' event shown in Figure 8. As stressed by *Frank and Ackerson* [1971], these bands of precipitation are encountered frequently and often are the principal contributors to the energy influx into the earth's upper atmosphere. These events are characterized by low average electron energies as the satellite initially enters the precipitation band, with a subsequent increase of average electron energy to a maximum and finally followed by a decrease to lower energies as the satellite passes through this band. This event as detected in the satellite survey mode of operation is depicted in the $E$-$t$ diagram (spectrogram) of Figure 8. The time $t_p$ for peak electron energy coincided with the encounter time $t_r$ for the peak of the electrostatic potential profile within the observational resolution of $\pm 12$ sec. We are currently correlating observations of high-time resolution to determine the relative encounter times within a resolution of $\pm 1$ sec. Relatively large convection electric fields, but not necessarily reversals of these fields, appear to be associated with inverted 'V' precipitation events. An example of the occurrence of such a precipitation event without a definite reversal but within a convection electric field $\sim 30$ mv $(\mathrm{m})^{-1}$ is shown in Figure 4 at 14h 51m 30s UT. (See also Figure 2 at 16h 27m 30s.)

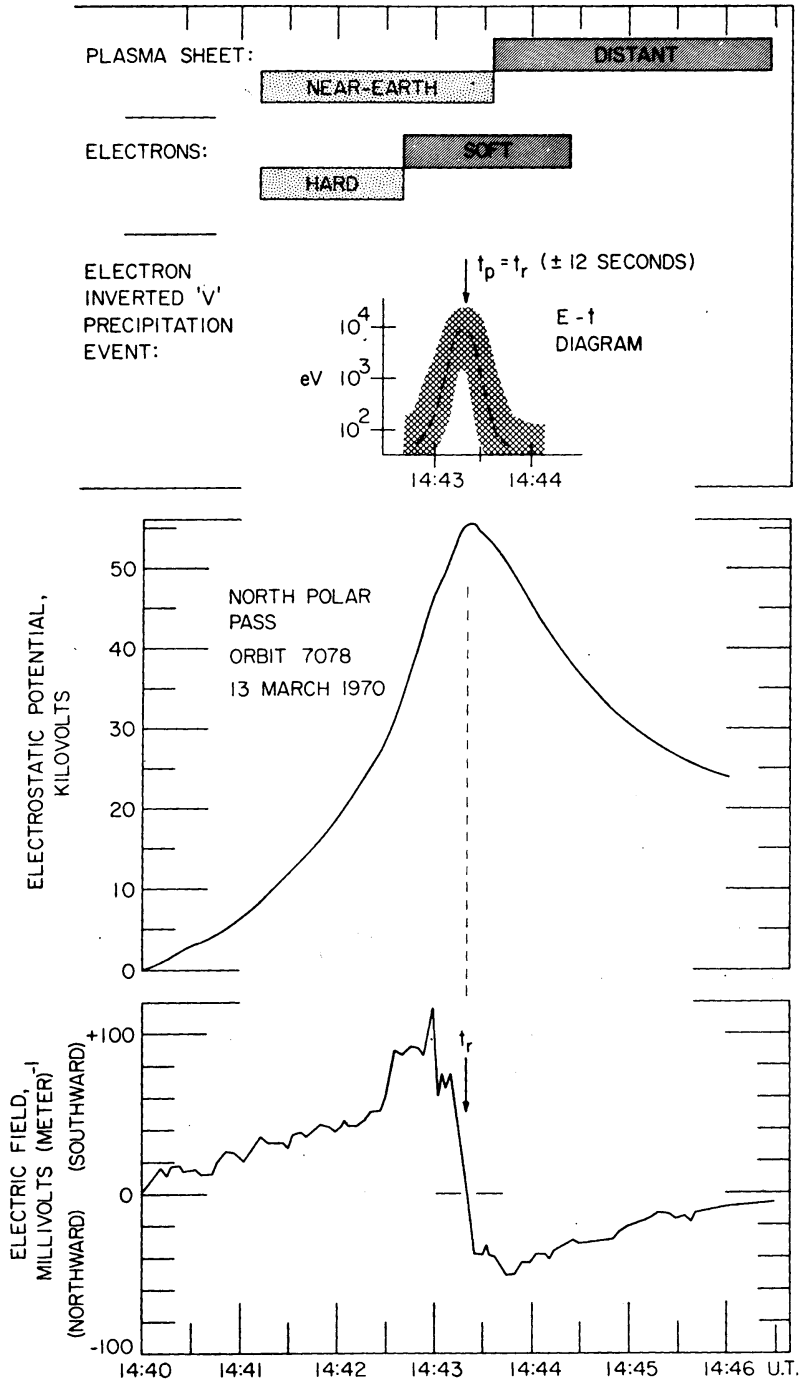


Fig. 8. Summary of several prominent features of convection electric fields and low-energy charged particle intensities as the satellite Injun 5 passed over an auroral arc centered at approximately 14h 43m 20s UT on March 13, 1970. (See also Figures 4, 5, and 6.)